Bioresource Technology 369 (2023) 128485

Contents lists available at ScienceDirect

Bioresource Technology

journal homepage: www.elsevier.com/locate/biortech

Integration of anaerobic digestion with heat Pump: Machine learning-based technical and environmental assessment

Zahra Hajabdollahi Ouderji [a,1], Rohit Gupta [a,b,c,1], Andrew Mckeown [a], Zhibin Yu [a], Cindy Smith [a], William Sloan [a], Siming You [a,*]

[a] James Watt School of Engineering, University of Glasgow, Glasgow G12 8QQ, UK
[b] Nanoengineered Systems Laboratory, UCL Mechanical Engineering, University College London, London WC1E 7JE, UK
[c] Wellcome/EPSRC Centre for Interventional and Surgical Sciences, University College London, London W1W 7TS, UK

HIGHLIGHTS

- Integration of air source heat pump with anaerobic digestion.
- Applying machine learning models to predict biogas and methane yield.
- Exploring the effects of heat pump operational parameters on biogas yield.
- Life cycle assessment application to investigate the environmental impacts.
- Proposed solution mitigates global warming potential significantly.

GRAPHICAL ABSTRACT

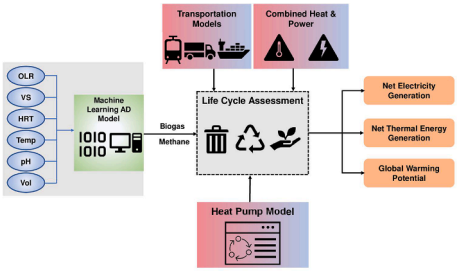

ARTICLE INFO

Keywords:
Net-zero
Bioenergy
Data-driven models
Life cycle assessment
Waste management

ABSTRACT

Anaerobic digestion (AD)-based biogas production mitigates the environmental footprint of organic wastes (e.g., food waste and sewage sludge) and facilitates a circular economy. The work proposed an integrated system where the thermal energy demand of an AD is supplied using an air source heat pump (ASHP). The proposed system is compared to a baseline system, where the thermal energy is supplied by a natural gas-based heating system. Several machine learning models are developed for predicting biogas production, among which the Gaussian Process Regression (GPR) showed a superior performance (R^2 = 0.84 and RMSE = 0.0755 L gVS^{-1} day^{-1}). The GPR model further informed a thermodynamic model of the ASHP, which revealed the maximum biogas yield to be approximately 0.585 L.gVS^{-1}.day^{-1} at an optimal temperature of 55 °C (thermophilic). Subsequently, life cycle assessment showed that ASHP-based AD heating systems achieved 28.1 % (thermophilic) and 36.8 % (mesophilic) carbon abatement than the baseline system.

1. Introduction

Over the past decades, anaerobic digestion (AD) has proven to be an effective way of reducing the volume of organic waste significantly, while recovering value-added products such as biogas and digestate. The performance of an AD process is strongly influenced by the choice of

* Corresponding author.
E-mail address: siming.you@glasgow.ac.uk (S. You).
[1] The authors contribute equally.

https://doi.org/10.1016/j.biortech.2022.128485
Received 30 October 2022; Received in revised form 9 December 2022; Accepted 11 December 2022
Available online 12 December 2022

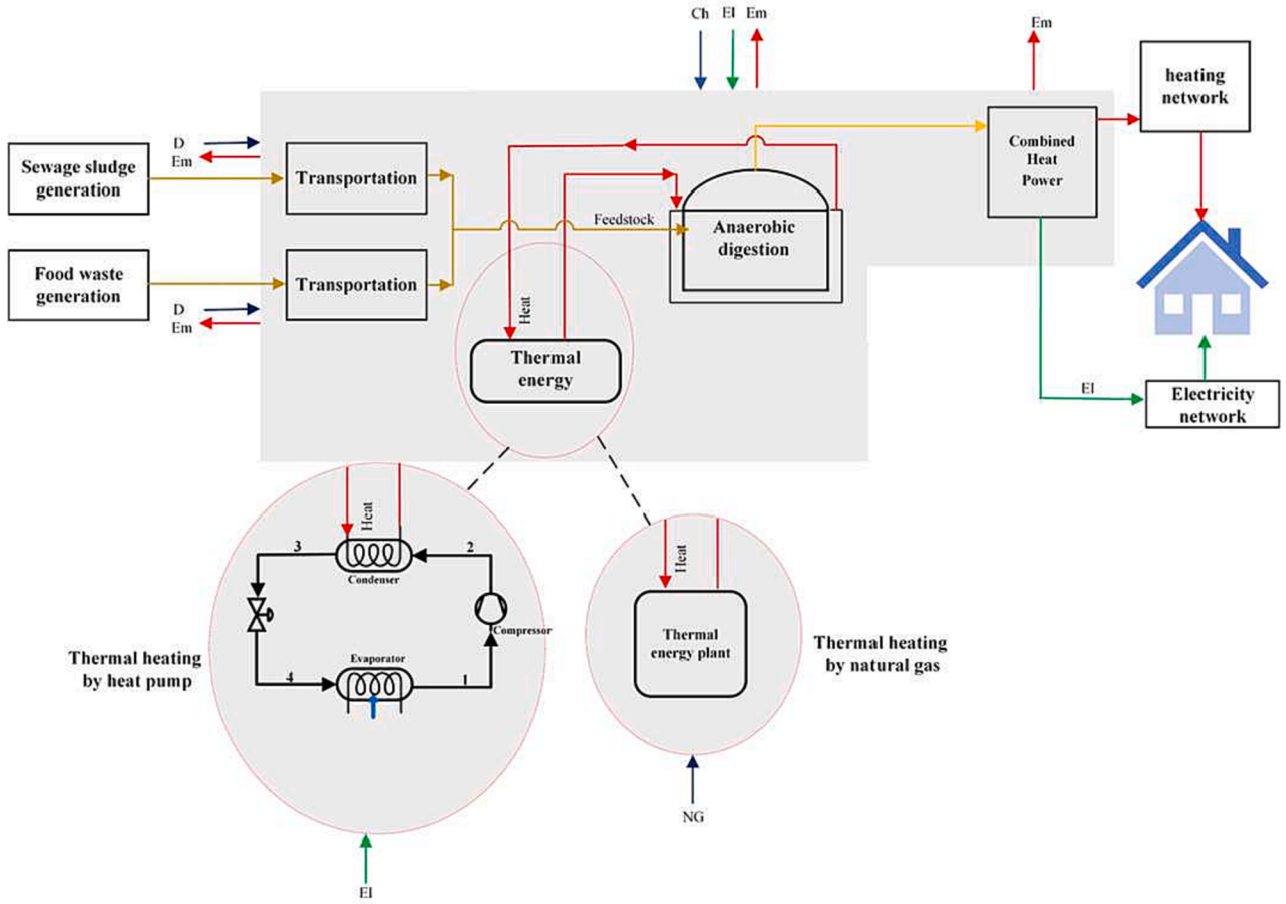

Fig. 1. Integration of the thermal systems with AD-CHP in for the baseline and alternative scenarios. The baseline scenario corresponds to a natural gas-based AD heating system, while the alternative scenario uses an ASHP-based heating system. Abbreviations – El: Electricity, D: Diesel, Ch: Chemicals, Em: Emissions. The grey shaded regions indicate processes that are included within the system boundary.

input waste which varies from vegetable and animal waste, agricultural waste to industrial and municipal solid waste, etc. Using multiple waste streams as a feedstock (co-digestion) is receiving increasing attention due to a higher biogas and methane production than that of the single feedstock AD processes (mono-digestion) (Pastor et al., 2013). Co-digestion is an efficient technique that balances the carbon-to-nitrogen (C/N) ratio, reduces the inhibitory effect of ammonia, and overcomes the disadvantages of mono-digestion (Karki et al., 2021; Polizzi et al., 2018). This further intensifies the fermentation process due to substrate nutrient balance, digesting the leftover materials and resulting in higher biogas production (Xu et al., 2018).

The AD process is also influenced by the choice of operating parameters such as pH, temperature, retention time, and solid content (Kothari et al., 2014). In terms of the temperature range of AD, there are psychrophilic (10–30 °C), mesophilic (30–40 °C), and thermophilic (50–60 °C) conditions (Sudiartha et al., 2022). At temperatures below 30 °C, the AD process becomes acidic, which is unfavourable for high biogas production. Similarly, at temperatures above 70 °C, the microbial communities (methanogenic bacteria) that facilitate the AD process are destroyed, which diminishes biogas production (Sun et al., 2022). It is seen that for temperatures higher than 45 °C, the amount of gas production monotonically increases (Sharma et al., 2022) and in the case of thermophilic bacteria, this temperature can increase up to 70 °C.

However, some of the studies argued that exploiting the monotonic increment of biogas by maintaining a temperature higher than 45 °C was not economically viable for several feedstocks, since maintaining this temperature would require significant thermal energy input. (Almomani, 2020). Similarly, in the psychrophilic range, the process is not economically viable due to limited biogas production. Therefore, tuning the operating temperature dynamically with changes in the input feedstock variation has been an everlasting challenge in AD process management (Nie et al., 2021).

AD systems are equipped with different types of heating systems with hot water or steam as the working fluid: (a) continuous passage of water through a heat exchanger installed outside the digester, (b) passage of hot water through heating coils installed inside the digester, (c) passage of hot water through the jacket around the digester, and (d) direct injection of steam into the AD. The required hot water or steam can be produced using (a) natural gas-fired boilers, (b) solar water heaters, or (c) biogas-fired boilers. Natural gas-fired boilers are the most common type of systems used in tandem with AD which has a significant economic and environmental footprint. On the other hand, the efficiency of solar energy-driven AD heating systems is strongly regulated by intermittency and geo-distributed availability of solar irradiance (Lombardi et al., 2020). For systems with biogas-fired boilers (or combined heat & power (CHP)), it is possible to supply the thermal energy required by AD by utilizing a fraction of the output biogas (Edwards et al., 2017; Evangelisti et al., 2014). However, deploying this system to an extreme climate with large seasonal temperature variations could drastically diminish the biogas output (thus heat and electricity) due to an abrupt increase in seasonal heating demand of AD. To circumvent these challenges, this work provides an alternative solution for supplying the thermal energy required by the AD using an air-source heat pump (ASHP), which is a low-carbon emission technology (Yu et al., 2022). Downstream to an AD plant, usually biogas-driven CHP plants are installed, which can simultaneously supply electricity and heat to the

central electricity grid and district heating network.

To study the performance of an ASHP-AD-CHP system, an accurate biogas (and methane) yield prediction model is essential, which can be achieved by data-driven AD modelling (Cruz et al., 2022). These models require preparing an *a priori* database, based on which they are trained. Following the training procedure, several unseen trial cases (test data) are subjected to the ML model, based on which the accuracy of the model is evaluated. A wide range of ML models has been developed for predicting biogas production from AD processes, among which artificial neural network (ANN) (Şenol, 2021), recurrent neural network (RNN) (Park et al., 2021), random forest (RF) (Wang et al., 2021), support vector machine (SVM) (Long et al., 2021), and extreme gradient boost (XGBoost) (Xu et al., 2021) have been popular choices among researchers. Therefore, the work compares the accuracies of five different ML models for predicting biogas yield and methane content for AD processes.

The optimal ML model informs the thermodynamic model of an ASHP and whole-system life cycle assessment (LCA) models, based on which the technological and environmental benefits of the ASHP-AD-CHP system are systematically evaluated. An exhaustive investigation is carried out which includes feature importance and parametric sensitivity analyses. The environmental benefit of the proposed integrated system is compared to a baseline AD-CHP operation system consisting of a natural gas-based heating system using LCA. To the best knowledge of the authors, this is a maiden attempt for integrating an ASHP with an AD system based on ML modelling, thermodynamic analysis, and LCA.

2. Material and methods

The technical feasibility and environmental benefits of retrofitting an AD system with ASHP is evaluated via thermodynamic analysis and LCA. An ML-based data-driven model of AD system using food waste and sewage sludge as feedstocks (Section 2.2) is coupled with a thermodynamic model of ASHP (Section 2.3). The data-driven and thermodynamic models together inform the input parameters for LCA (Section 2.4) to quantify the environmental benefits of the proposed solution.

2.1. System-level integration of heat pump with anaerobic digester

For different input waste compositions, the AD process should be kept within a temperature range between 30 and 55 °C to ensure optimal biogas production. Since the input temperature of the waste is usually always lesser (within the range of 10–20 °C) than the temperature range of AD reactor, additional thermal energy is required to elevate the temperature of the waste stream (thus enhancing the microbial activity). In usual practice, the thermal energy required by AD is resourced from a central thermal energy production plant driven by natural gas (see Fig. 1).

The alternative scenario incorporates an HP, which is an environment-friendly technology with a potential to reduce dependence on the fossil fuel sector. ASHP attracts significant attention among the other categories of HPs (such as water source and geothermal) due to its simpler configuration and lower initial cost. In addition, ASHP has high heating potential in cold-climate and is characterized by energy-saving potential, while being operationally reliable. By using HP, the heat released in the condenser is utilized to heat the external fluid which is applied as the heat agent for the heating purpose of AD as shown in Fig. 1. In fact, AD acts as a thermal storage tank and absorbs the heat that is rejected from the HP. For different operation temperatures of AD, the condenser heat capacity is calculated to provide the required heat for the digester. According to the condenser heat, the refrigerant mass flow rate of the ASHP is calculated, and by having the mass flow rate, compressor power consumption and system COP are consequently obtained using Eq. (10).

The main product of AD is biogas which has a significant percentage of methane and can be used as a combustible material in various industries to produce electricity and heat. By installing an onsite CHP, the AD-generated biogas is further converted to thermal energy and electricity, which can partially displace the load on the central grid. Therefore, by performing the AD process, it is possible to reduce the volume of sludge, and use the resulting biogas for energy production.

Table 1
Statistics of the databases for developing biogas yield and methane content prediction models containing 167 and 91 datasets, respectively.

Biogas yield prediction model database					
Type	Variable	Min	Max	Average	SD
Inputs	OLR (gVS L^{-1} day^{-1})	0.04	16.15	3.46	2.89
	VS (wt.%)	1.58	35.26	9.59	6.76
	Temperature (°C)	20	56	39.9	8.15
	HRT (day)	4	100	28.67	17.64
	pH	6.4	8.3	7.55	0.40
	Reactor volume (L)	0.1	64	9.22	12.14
Output	Biogas yield (L gVS^{-1} day^{-1})	0.16	0.97	0.55	0.19
Methane content prediction model database					
Type	Variable	Min	Max	Average	SD
Inputs	OLR (gVS L^{-1} day^{-1})	0.37	19.7	4.27	3.74
	VS (wt.%)	1.43	35.26	8.38	6.98
	Temperature (°C)	35	56	43.75	9.01
	HRT (day)	3	100	25.65	16.83
	pH	6.61	8.3	7.6	0.32
	Reactor volume (L)	0.1	30	5.95	5.25
Output	Methane content (%)	40.3	78.	61.17	6.71

2.2. Machine learning model for anaerobic digestion

2.2.1. Data assimilation

Being a multi-step multi-physics biokinetic process, developing an intricate model for AD is highly complex. The work herein requires prediction of biogas production rate and percentage of methane within biogas by deploying a model for AD. To achieve this, a data-driven model is developed based on the data obtained from the literature that includes a wide range of food waste and sewage sludge as AD feedstock. A total of 167 biogas yield and 91 methane percentage datasets are obtained from the literature (see Supplementary Material). It is important to note that these datasets only represent the low-solid AD (i.e., total solids (TS) < 25 wt.%). Since the ML model is to be integrated with an ASHP thermodynamic model, the primary criterion for shortlisting relevant literature is that it must report the operating temperature, which limits the size of the dataset. Additionally, the mismatch between the size of biogas yield and methane percentage datasets is due to the inconsistency in output variable reporting within the collected datasets. While one can incorporate a large variety of input variables for constructing the database, it is not practically feasible to gather data from the literature for each of them. Therefore the following variables are chosen based on their frequency of reporting and importance in regulating biogas (and methane) yields: (1) organic loading rate (OLR) in gVS L^{-1} day^{-1}, (2) volatile solid (VS) in wt.%, (3) reactor temperature in °C, (4) hydraulic retention time (HRT) in days, (5) pH, (6) reactor volume in L, (7) biogas generation in L gVS^{-1} day^{-1}, and (8) methane content in biogas expressed in vol.%. Out of these eight attributes, the first six are to be used as input variables (or predictor) to the data-driven models, while the latter two are the output variables (or predicted). It is inevitable that the constructed dataset still contains missing values of input features. This is addressed by the mean imputation of missing value for facilitating a mean regression model development, which is a common practice in data-driven bioprocess modelling (Ascher et al., 2022a). A statistical summary of these attributes across the entire datasets is provided in Table 1. Since the dataset contains attributes of different range and central tendency, a normalization step is required to be applied before being fed into the data-driven model. Following a prior ML work (Li et al., 2022), the standard normal variate (Z_i) is used

for this purpose, defined as $Z_i = (X_i - \mu)/\sigma$. Here X_i is the data series for i^{th} variable, μ and σ are the mean and standard deviation of the data series corresponding to the i^{th} variable.

To gain a better sense of nonlinear relationship among any two variables in the parametric space, the Spearman Correlation Coefficient (SCC), a nonlinear statistical metric is selected and defined as (Ascher et al., 2022a),

$$\mathrm{SCC} = \frac{\sum_{i=1}^{N}\{R(x_i) - \overline{R(x)}\}\{R(y_i) - \overline{R(x)}\}}{\sqrt{\sum_{i=1}^{N}\{R(x_i) - \overline{R(x)}\}^2}\sqrt{\sum_{i=1}^{N}\{R(y_i) - \overline{R(y)}\}^2}} \quad (1)$$

Here, the total length of data points is N, $R(x_i)$ and $R(y_i)$ are the rank of each sample for the variables of interest, and $\overline{R(x)}$ and $\overline{R(y)}$ are the average ranks of the two variables. An SCC value of zero suggests that the variables are uncorrelated, while SCC $= \pm 1$ suggests the strongest possible correlation between the variables. The result obtained from SCC analysis is visualized via a two-dimensional heatmap in Section 3.1.

2.2.2. Model development

Two data-driven models are developed where the first predicts biogas production in L gVS^{-1} day^{-1}, while the latter predicts percentage of methane content in biogas. Each model is provided with six inputs: OLR, VS, HRT, reactor temperature, pH, and volume. The ML models are implemented based on the *Regression Learner Toolbox* in the MATLAB R2021b environment. Five different types of data-driven ML methods such as Neural Network (NN), Support Vector Machine (SVM), Gaussian Process Regression (GPR), Tree, and Ensemble are explored to predict the two output variables of AD. The MATLAB toolbox enables automatic hyperparameter optimization based on the Bayesian Optimization method (iterations = 30), which provides the best set of hyperparameters for each ML algorithm. Each of the databases was randomly split into two parts (a) 12.5 % for testing and (b) 87.5 % for training/validation. With the training/validation dataset, a 5-fold cross-validation was performed to ensure model generalizability and optimal fitting.

The first method, NN, is a widely used non-linear ML algorithm that creates a computational graph consisting of input, output, and hidden layers. Essential hyperparameters search ranges adopted by the toolbox are number of fully connected layer: 1–3; activation function: ReLU, Tanh, Sigmoid; regularization strength (Lambda): 5.988×10^{-8}–5.988×10^{2}; and neurons in each layer: 1–300.

The second method SVM is a non-parametric non-linear non-probabilistic method, that relies on mapping the input features into a high-dimensional space using a non-linear kernel function. Subsequently it creates an optimal hyperplane to differentiate between various subsets. Important SVM hyperparameters search ranges in the MATLAB toolbox are box constraint: 0.001–1000; kernel scale: 0.001–1000; Epsilon: 0.00021868–21.8681; and kernel function: Gaussian, Linear, Quadratic, and cubic.

The third algorithm GPR is a non-linear, non-parametric, Bayesian probabilistic data-driven method specifically suitable for datasets with high variances. An additional incentive offered by GPR is the information about predictive uncertainty of the model output variable, which is absent for most of the other non-probabilistic data-driven methods. Essential GPR hyperparameters ranges considered in the toolbox are Sigma: 0.0001–1.9087; basis function: Constant, Zero, Linear; kernel function: Nonisotropic Exponential, Nonisotropic Matern 3/2, Nonisotropic Matern 5/2, Nonisotropic Rational Quadratic, Nonisotropic Squared Exponential, Isotropic Exponential, Isotropic Matern 3/2, Isotropic Matern 5/2, Isotropic Rational Quadratic, Isotropic Squared Exponential; and kernel scale: 0.096–96.

The fourth method is the tree-based algorithm, constructed of nodes (or leaves) and branches, which are routinely used for solving regression problems. The hyperparameter search range responsible for this algorithm is minimum number of leaves: 1–83. The fifth algorithm is the ensembles of trees, which uses several trees constructed in series or parallel, which circumvents simplicity and overfitting problems experienced by single tree-based algorithms. Optimizable ranges for hyperparameters for the ensemble-based method are ensembling method: Bag, Least Square Boost (LSBoost); number of learners: 10–500; learning rate: 0.001–1; minimum leaf size: 1–83; and number of predictors to sample: 1–6. Based on the description of hyperparameter ranges for various data-driven methods, the Bayesian optimization algorithm yields the five best possible combinations of hyperparameters with optimal regression fitting.

2.2.3. Accuracy metrics and feature importance

For examining the degree of accuracy and degree of fitting for a regression-based problem several metrics are essential to be considered such as: mean squared error (MSE), mean absolute error (MAE), root mean squared error (RMSE), and coefficient of determination (R^2) defined as follows.

$$\mathrm{MSE} = \frac{\sum_{i=1}^{N}\left(y_i^{true} - y_i^{pred}\right)^2}{N} \quad (2)$$

$$\mathrm{MAE} = \frac{\sum_{i=1}^{N}\left|y_i^{true} - y_i^{pred}\right|}{N} \quad (3)$$

$$\mathrm{RMSE} = \sqrt{\frac{\sum_{i=1}^{N}\left(y_i^{true} - y_i^{pred}\right)^2}{N}} \quad (4)$$

$$\mathrm{R}^2 = 1 - \frac{\sum_{i=1}^{N}\left(y_i^{true} - y_i^{pred}\right)^2}{\sum_{i=1}^{N}\left(y_i^{true} - y_{avg}^{pred}\right)^2} \quad (5)$$

where y_i^{true} and y_i^{pred} are the true and predicted values of output variable, respectively, and y_{avg}^{pred} is the average of all the predicted values of an output variable.

In addition to accuracy metrics, quantifying the interpretability of a data-driven model is essential. In this work, the interpretability of the model is assessed by conducting the feature importance via Shapley Additive Explanation (SHAP) metric, a game theory-based model output explainer (Ascher et al., 2022b). The SHAP values obtained from the data-driven model are represented in terms of average feature importance (AFI) using the following expression,

$$\mathrm{AFI} = softmax(|\mathrm{mean}(\mathrm{SHAP})|) \quad (6)$$

where the *softmax* function converts the average of absolute SHAP values (i.e., $|\mathrm{mean}(\mathrm{SHAP})|$) to a range between 0 and 1.

2.3. Thermodynamic model of air source heat pump

An ASHP consists of a compressor (process 1–2), a condenser (process 2–3), an expansion device (process 3–4), and an evaporator (process 4–1) as shown in Fig. 1. The low-pressure vapour refrigerant at point 1 is compressed to the point 2 where the temperature is increased, and pressure reaches a condensation level. The high temperature vapour exiting the compressor de-superheats and condenses in the condenser and its temperature decreases at point 3 (heat Q_C is released). The high-temperature and high-pressure liquid refrigerant leaving the condenser is then throttled via the expansion valve to reach the evaporator temperature at point 4. The produced two-phase mixture then fully evaporates in the evaporator by absorbing heat from a heat source Q_E (e.g., outdoor air) and returns to the compressor for circulation (Yu et al., 2022). The model assumption are: (a) each equipment in the system is operated at steady-state condition; (b) pressure loss is neglected in the evaporator and condenser; (c) compressors are considered as isentropic with efficiency of 100 %; (d) refrigeration state at point 1 and 3 is

saturated vapor and saturated liquid, respectively; (e) heat transfer in the heat exchanger equipment is isothermal; (f) The integrated system is operated under the steady-state condition; and (g) the AD is well insulated and heat loss from the digestion is considered negligible.

To simulate the ASHP cycle, each component is considered as a control volume. Using the energy and mass balance for each component the governing equations are obtained. As observed in Fig. 1, the condenser heat load ($\dot{Q}_C$) is calculated as,

$$\dot{Q}_C = \dot{m}(h_2 - h_3) \tag{7}$$

where $\dot{m}$ is the mass flow of refrigerant, h is the specific enthalpy. The rejected heat in the condenser is absorbed to provide the heat demand of the AD process. The heat transfer rate ($\dot{Q}_E$) of the evaporator is expressed as,

$$\dot{Q}_E = \dot{m}(h_1 - h_4) \tag{8}$$

where subscript E is used to denote the evaporator. Similarly, the compressor power consumption is ($\dot{W}_{Comp}$) is defined as,

$$\dot{W}_{Comp} = \dot{m}(h_2 - h_1) \tag{9}$$

Here subscripts 1 to 4 represent the numbering of the state points shown in Fig. 1. Consequently, the coefficient of performance (COP) in the ASHP is calculated as:

$$\mathrm{COP} = \frac{\dot{Q}_C}{\dot{W}_{Comp}} \tag{10}$$

It is important to note that for all the simulation cases, the evaporator temperature is fixed to 0 °C. The entire model is implemented in MATLAB R2021a and linked to the REFPROP v9.0 database, which contain the thermodynamic properties (such as enthalpy, entropy, temperature, pressure) of the refrigerants. The COP of the ASHP for a range of evaporator temperatures is benchmarked using a related literature (Baskaran and Mathews, 2015) (see supplementary material).

2.4. Life cycle assessment

2.4.1. Goal, Scope, and functional unit

The goal of the LCA adopted in this work is to perform a comparative assessment between a baseline AD system located in the United Kingdom provided with thermal energy generated with natural gas to an alternative scenario where the required heat is provided using an ASHP described in the previous section. The scope of the LCA framework includes sub-processes such as transportation of feedstock to AD plant, modelling of AD process that intakes food waste and sewage sludge as feedstock, modelling of a biogas-driven CHP plant, and supplying CHP-generated energy content to the central electricity and heating grid. In addition to biogas, the AD plant generates digestate as a by-product, whose utilization or disposal is excluded from this study. Here, 1 wet tonne of feedstock is assigned as the functional unit (FU). The framework follows the guideline provided by ISO 14,040 and is implemented within a commercial LCA software GaBi (Gupta et al., 2022a).

2.4.2. Life cycle inventory and process models

The hypothetical AD system is fed with two types of feedstocks, out of which 60% is food waste and 40% is sewage sludge (Kesharwani and Bajpai, 2020). Therefore, within the FU of 1 tonne feedstock, 600 kg is food waste and 400 kg is the sewage sludge. Two separate truck processes implemented in GaBi (US: Truck - Dump Truck/52000 lb payload) transport these two waste streams over a 20 miles distance to the AD plant. The diesel consumptions for the transportation process are modelled via the GaBi process GB: Diesel mix at refinery.

The AD plant requires electricity, chemical, and heat as valuable inputs to produce biogas as the major value-added product and off-gas emissions. The electricity required by the AD is modelled using the GB: Electricity grid mix process. An essential chemical required for the AD process is polyacrylamide, which is modelled using the GaBi process EU-28: Polyamide 6 (PA6). The heat required by the AD plant depends on the operating temperature of the AD reactor and is given by the following equation.

$$Q_{AD} = m_{FS} C_{p,FS} (T_{AD} - T_{FS}) \tag{11}$$

where m_{FS} is the mass flow of feedstock (1 tonne of waste per year), $C_{p,FS}$ is the specific heat capacity at constant pressure for the mixed waste, T_{AD} is the operating temperature of AD (i.e., 37.5 °C for mesophilic condition and 55 °C), and T_{FS} is the temperature at which the feedstock enters the AD reactor (assumed as 15 °C for UK-based scenario). The $C_{p,FS}$ for the mixed waste stream containing 60 % food waste and 40 % sewage sludge is calculated as 3.71 KJ $kg^{-1}K^{-1}$ based on the data obtained from literature (Kesharwani and Bajpai, 2020).

The heat required by the AD i.e., Q_{AD} is supplied by two mechanisms in the LCA framework: (a) for the conventional scenario the heat is supplied from grid which is generated from natural gas (modelled using GaBi process GB: Thermal energy from natural gas) and (b) for the alternative scenario the heat is supplied by an on-site installed ASHP, whose COP depends on the operating temperature. The electricity required by the HP in the alternative scenario is modelled using GB: Electricity grid mix. The biogas produced by the AD reactor under varying temperature and other input conditions are calculated using the ML model described in earlier sections. The direct emissions for the AD systems such as carbon dioxide and methane caused by biogas leakage are obtained from a relevant literature (Ascher et al., 2020).

The biogas produced by the AD is further fed to an onsite CHP system producing electricity and heat simultaneously, which ultimately is supplied to the grid. The following equations describe the electricity (E_{gen}) and heat (Q_{gen}) production from biogas.

Table 2
Life cycle inventory used for conducting the analysis in GaBi software.

Quantity	Value (unit)	Reference
Food waste	60 % of FU i.e., 0.6 t	(Kesharwani and Bajpai, 2020)
Sewage Sludge	40 % of FU i.e., 0.4 t	(Kesharwani and Bajpai, 2020)
Distance of feedstock generation site to AD plant	20 miles	Assumed
Polyacrylamide (for AD plant)	0.429 kg/t AD feedstock	(Edwards et al., 2017)
Electricity (for AD plant)	15.4 kWh/t AD feedstock	(Edwards et al., 2017)
Thermal energy for AD plant with 37.5 °C operating scenario	83.5 MJ/t AD feedstock	Calculated
Thermal energy for AD plant with 55 °C operating scenario	148.4 MJ/t AD feedstock	Calculated
Direct CH_4 emissions (for AD plant)	10.855 g/kg biogas	(Ascher et al., 2020)
Direct CO_2 emissions (for AD plant)	16.118 g/kg biogas	(Ascher et al., 2020)
Biogas generation for AD plant operating at 37.5 °C	4.22 kg/t AD feedstock	Calculated
Biogas generation for AD plant operating at 55 °C	7.35 kg/t AD feedstock	Calculated
Direct CO emissions (for CHP plant)	2.16 g/kg biogas	(Ascher et al., 2020)
Direct CH_4 emissions (for CHP plant)	8.72 g/kg biogas	(Ascher et al., 2020)
Direct NO emissions (for CHP plant)	2.78 g/kg biogas	(Ascher et al., 2020)
Direct NMVOC emissions (for CHP plant)	1.97 g/kg biogas	(Ascher et al., 2020)
Particulate matter (2.5–10 μm) emissions (for CHP plant)	0.72 g/kg biogas	(Ascher et al., 2020)
Electricity consumption of the HP for 37.5 °C AD operation scenario	4.49 kWh/t AD feedstock	Calculated
Electricity consumption of the HP for 55 °C AD operation scenario	10.68 kWh/t AD feedstock	Calculated

$$Q_{gen} = \frac{\eta_{el}^{CHP} m_{BG} CV_{BG}}{\rho_{BG}} \quad (12)$$

$$E_{gen} = \frac{\eta_{th}^{CHP} m_{BG} CV_{BG}}{\rho_{BG}} \quad (13)$$

In addition, the CHP causes a significant amount of direct emissions to the air which includes carbon monoxide, methane, nitrogen oxide, non-methane volatile organic carbon (NMVOC), and particulate matter (Ascher et al., 2020). In Eqs. (13) and (14) $\eta_{th}^{CHP} = 0.5$ is thermal efficiency of CHP, $\eta_{el}^{CHP} = 0.33$ is the electrical efficiency of CHP, $CV_{BG} = 23$ MJ m^{-3} is the net calorific value of biogas, $\rho_{BG} = 1.2$ kg m^{-3} is the density of biogas, and m_{BG} is the mass of biogas entering into the CHP. Given the AD operating and feedstock conditions, the ML model determines the mass of biogas generated that enters the CHP. The value-added products generated by the CHP system offsets the environmental footprint of the total system by supplying electricity and heat to the grid. These emission offsets are calculated using the emissions factors provided by the UK government as 0.212 $kgCO_2$-eq/kWh for electricity and 0.203 $kgCO_2$-eq/kWh for natural gas. This calculation assumes that using heat is analogous to consumption of natural gas. The life cycle inventory (LCI) is provided in Table 2.

2.4.3. Life cycle impact assessment

The relative benefits of the two different scenarios i.e., AD with HP and AD with natural gas-based heating, the GWP metric is considered expressed in terms of $kgCO_2$-eq/t feedstock added to the AD. The GWP is evaluated using the CML 2001-August 2016 methodology (Gupta et al., 2022a) and measured in terms of GWP over 100 years (i.e., GWP100), which is in accordance with the IPCC norms. It is important to note that the biogenic CO_2 is excluded from the LCA framework, which is consistent with a prior work (Gupta et al., 2022b).

2.4.4. Data interpretation

Following the LCIA described in Section 2.4.3, the environmental impact (i.e., GWP) for AD systems resources resourced with thermal energy from (a) natural gas and (b) heat pump is compared. For each scenario, two cases are considered which incorporates two different operating conditions of the AD process (Section 3.3). In addition, a one-way sensitivity analysis is performed to examine the individual influence of parameters on the GWP. The sensitivity ratio for i^{th} parametric change (SR_i) is considered defined as,

$$SR_i = \frac{\left|\frac{GWP_i^{baseline} - GWP_i^{modified}}{GWP_i^{baseline}}\right|}{\left|\frac{\Phi_i^{baseline} - \Phi_i^{modified}}{\Phi_i^{baseline}}\right|} \quad (14)$$

where Φ_i and GWP_i are the value of i^{th} parameter and the GWP corresponding to that. Some of the essential parameters considered in the sensitivity analysis are thermal and electrical efficiencies of the CHP unit, electricity and polyacrylamide consumption of the AD, waste transportation distance, biogas generation, temperature of the AD input feedstock, and COP of the ASHP.

3. Results and discussion

3.1. Performance and interpretability of data-driven models

The accuracy metrics such as RMSE, R^2, MSE of five different ML models (GPR, ensembles of trees, NN, tree, and SVM) developed to predict biogas production and methane content in biogas are provided in Table 3. In addition, the prediction speed in observations per second and the model training time in seconds are provided. A high-level inspection of Table 3 reveals that the GPR outperforms all other ML models for predicting both biogas production and methane content in biogas. For the GPR-based biogas yield prediction model $R^2 = 0.84$ and RMSE =

Table 3
Performance of various data-driven models investigated for constructing the biogas yield (L gVS^{-1} day^{-1}) and methane content in biogas (%) prediction models. The rank is provided based on R^2 and RMSE values.

Output variable	Model Type	Optimal Hyperparameters	RMSE	R^2	MSE	MAE	Prediction Speed (Obs/*sec*)	Training Time (*sec*)
Biogas yield (L gVS^{-1} day^{-1})	GPR	Basis function: constant, kernel function: nonisotropic squared exponential, kernel scale: 1.1254, sigma: 0.028, standardize data: true)	0.0755	0.84	0.0057	0.057	20,000	18.731
	Ensemble of Trees	Ensemble method: least square boost, minimum leaf size: 2, number of learners: 47, learning rate: 0.032, number of predictors to sample: 6)	0.0819	0.82	0.0067	0.062	5400	30.686
	NN	Fully connected layers: 2, activation: ReLU, iteration limit: 1000, regularization strength: 0.0003, standardize data: true, 1st layer size: 100, 2nd layer size: 290)	0.1060	0.69	0.0112	0.071	14,000	58.765
	Tree	Surrogate decision splits: off, minimum leaf size: 2)	0.1172	0.62	0.0137	0.087	17,000	11.333
	SVM	Type: fine Gaussian, kernel function: Gaussian, kernel scale: 0.61, box constraint: automatic, epsilon: automatic, standardize data: true)	0.1174	0.62	0.0138	0.091	26,000	0.0281
Methane content in biogas (%)	GPR	Basis function: constant, kernel function: nonisotropic matern 3/2, kernel scale: 0.3016, sigma: 0.0056, standardize data: true)	1.4575	0.82	2.1244	0.7839	19,000	18.648
	Ensemble of Trees	Ensemble method: bag, minimum leaf size: 1, number of learners: 500, number of predictors to sample: 4)	1.9081	0.69	3.6410	1.1240	540	101.73
	Tree	Surrogate decision splits: off, minimum leaf size: 4)	2.5543	0.45	6.5243	1.4735	25,000	9.678
	SVM	Kernel function: Gaussian, kernel scale: 2.22, box constraint: 43.492, epsilon: 0.461, standardize data: false	2.5962	0.43	6.7403	1.7228	26,000	23.798
	NN	Fully connected layers: 3, activation: sigmoid, iteration limit: 1000, regularization strength: 0.0189, standardize data: yes, 1st layer size: 91, 2nd layer size: 1, 3rd layer size: 3)	2.9885	0.25	8.9309	2.0571	18,000	37.502

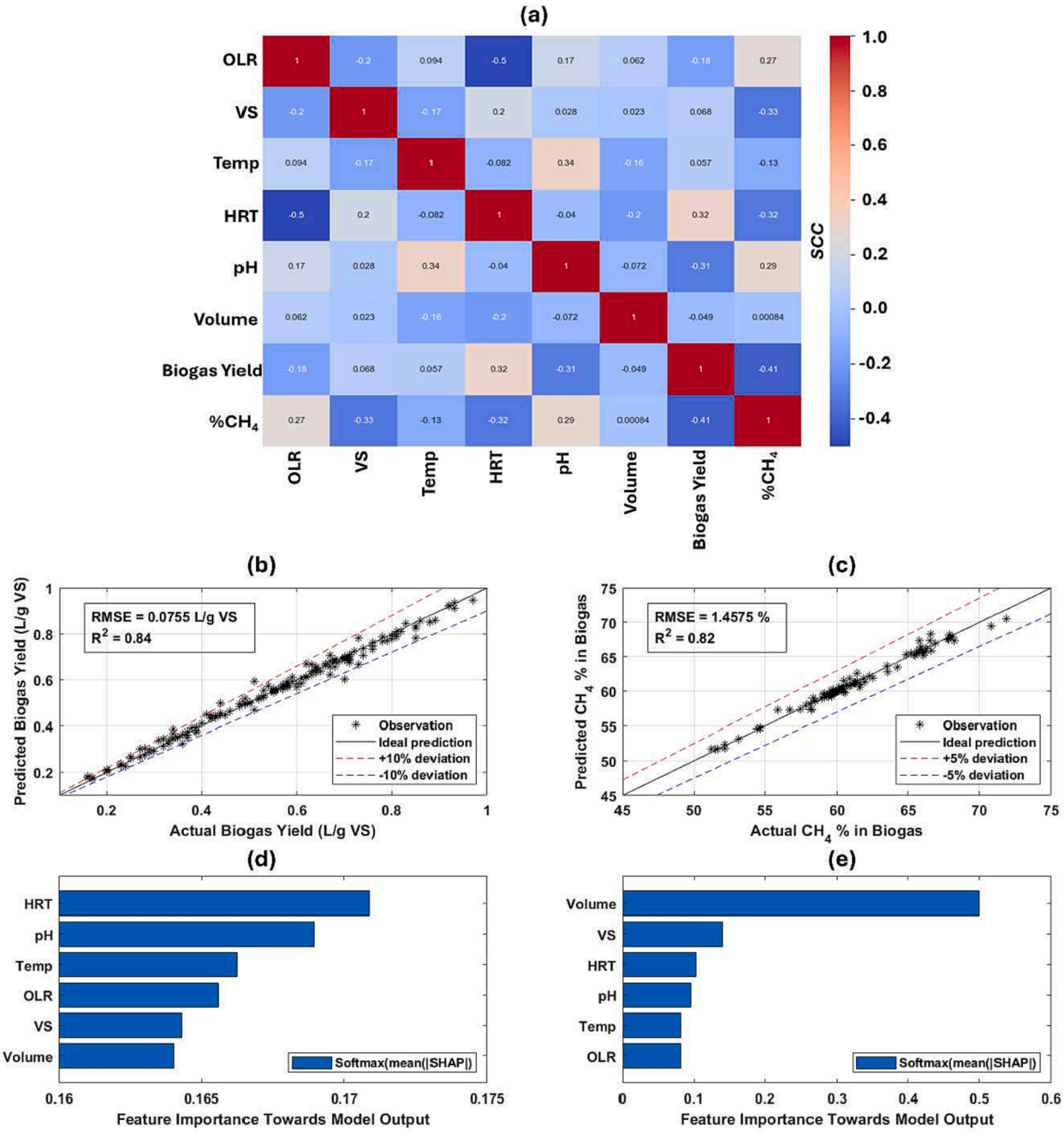

Fig. 2. Results for the data-driven models associated with AD of food waste and sewage sludge: (a) Spearman Correlation Coefficients between any two variables of interest, (b) and (c) Parity plots showing performance of the optimal biogas yield and methane percentage prediction models evaluated based on testing dataset, (d) and (e) Feature importance analysis for biogas yield and methane percentage prediction models via SHAP value quantification. The quantities shown in the feature importance maps correspond to Softmax function-normalized mean of absolute SHAP values, showing relative importance of input features towards predictions of output variables (biogas yield and methane percentage).

0.0755 L gVS^{-1} day^{-1}. Similarly, the GPR-based methane content prediction model has $R^2 = 0.82$ and RMSE = 1.4575 %. To test the significance level of the GPR model predictions, the F-statistic score is used, given by,

$$F = \frac{R^2(N-k)}{1-R^2(k-1)} \tag{15}$$

where N is the number of samples (167 and 91 for biogas yield and methane content models, respectively), $k = 6$ is the number of independent parameters. The R^2 values for biogas yield and methane content models are 0.84 and 0.82 (see Table 3). This leads to F-statistic scores for biogas yield and methane content models to be 91.9 and 42.6. Referring to the F-table these correspond to the probability value (p-value) of zero, suggesting that the GPR model correctly predicts the data trend (i.e., the correlation is highly significant). The predictive accuracy of the optimal model is competitive with those reported in the literature of ML-based AD modelling with R^2 in the range of 0.8 to 0.9 (Cruz et al., 2022; Long et al., 2021; Wang et al., 2021; Xu et al., 2021). This superior performance of the GPR model when compared to other models is attributed to the capability of probabilistic Gaussian processes to handle datasets with a high degree of variance (see Table 3). Therefore, non-probabilistic, yet kernelized (e.g., SVM) or non-kernelized (e.g., NN, tree, ensembles) methods suffer inferior predictive accuracies under

Table 4
Waste characteristics of two cases considered for the parametric sensitivity analyses.

Parameters	Thermodynamic Sensitivity Analysis		LCA	
	Case 1	Case 2	Case A	Case B
OLR (gVS L^{-1} day^{-1})	5	1	1.65	3.42
VS (wt.%)	15	30	1.2	2.5
HRT (days)	20	15	30	20
pH	7.5	7.5	7.5	7.7
Volume (L)	20	20	20	20
Optimal Temperature (°C)	37.5	55	37.5	55

such scenarios. For further model interpretability analysis, thermodynamic assessment, and LCA, the GPR-based models are used.

The two-dimensional heatmap shown in Fig. 2a describes the correlation between any two variables utilized for developing the ML models based on the SCC (see Eq. (1)). In this work |SCC|⟩0.1 is designated as a significant correlation between the inputs and outputs. It is observed that the biogas yield is strongly correlated with AD several input variables such as HRT, pH, and OLR, which are consistent with the explainable ML-based AD literature (Long et al., 2021; Wang et al., 2021). Although other influential factors such as C/N ratio, volatile fatty acid (VFA), etc. can strongly influence the biogas yield, they were excluded from this modelling framework due to the inconsistency in their reporting in the literature (Cruz et al., 2022). In contrast, the methane percentage in biogas is strongly correlated with VS HRT, OLR, temperature, and pH, which has been observed by existing studies for long-term industrial-scale co-digesters (Wang et al., 2021). Although the |SCC| can indicate the correlation between various features and predictor variables, they donot descibe the model behavior. For this purpose, model-agnostic interpretability metrics, such as SHAP score are used in this work (see Eq. (6)). The parity plots showing the efficacy of the GPR-based biogas yield and methane fraction prediction models are shown in Fig. 2b and c. Most of the model predictions are within the 10% prediction error band for the biogas yield and well-within the 5% error band for the methane percentage models, further confirming the accurate choice of the ML model. The explainability of the GPR model is shown in Fig. 2d and e, describing the competitive influence of input features towards altering the output variables. The Figure shows feature importance values calculated via Eq. (6), which is dependent on the *softmax*-normalized mean SHAP score, a routinely used metric (Ascher et al., 2022b). For biogas yield model the features with top three SHAP scores are HRT, pH, and temperature, suggesting that any alteration or uncertainty associated with these metrics will strongly influence the accuracy of GPR-based ML model. For the methane percentage model, the features with top three SHAP scores are reactor volume, VS, and HRT. Although the present work does not include partial dependence analysis, it will be an essential contribution in future to understand the functional correlation between top input features and the output variable.

3.2. Parametric sensitivity analysis

For ensuring an optimal set of operating parameters and type of refrigerant choice that will provide maximum heating for the AD system at minimum energy consumption, a rigorous parametric study is essential. For this purpose, two cases of waste compositions and AD operating parameters were considered. It is important to note that the AD operational temperature needs to be adjusted as per the input waste stream composition so that the biogas yield is maximized. The details for these cases are shown in Table 4 and are used as input parameters to calculate the biogas yield using the optimal ML model (i.e., GPR). The influences of the following attributes are investigated: (a) choice of refrigerant, (b) condenser temperature, (c) mass flow of refrigerant, and (d) evaporator temperature.

3.2.1. Refrigerant selection

Six different types of popularly used refrigerants are investigated as working fluid for the ASHP: R134a, R1234ze, R32, R290, R717 (ammonia), and R410. As shown in Table 4 the optimal AD temperature corresponding to the waste streams for Cases 1 and 2 are 37.5 and 55 °C, respectively. The values for biogas and methane yields for Case 1 are 0.568 and 0.342 L gVS^{-1} day^{-1}, while those for Case B are 0.584 and 0.351 L gVS^{-1} day^{-1}, respectively. These values are determined by the optimal ML model (i.e., GPR) and suggest that increasing the AD temperature as per the input waste composition, can enhance both biogas and methane yields.

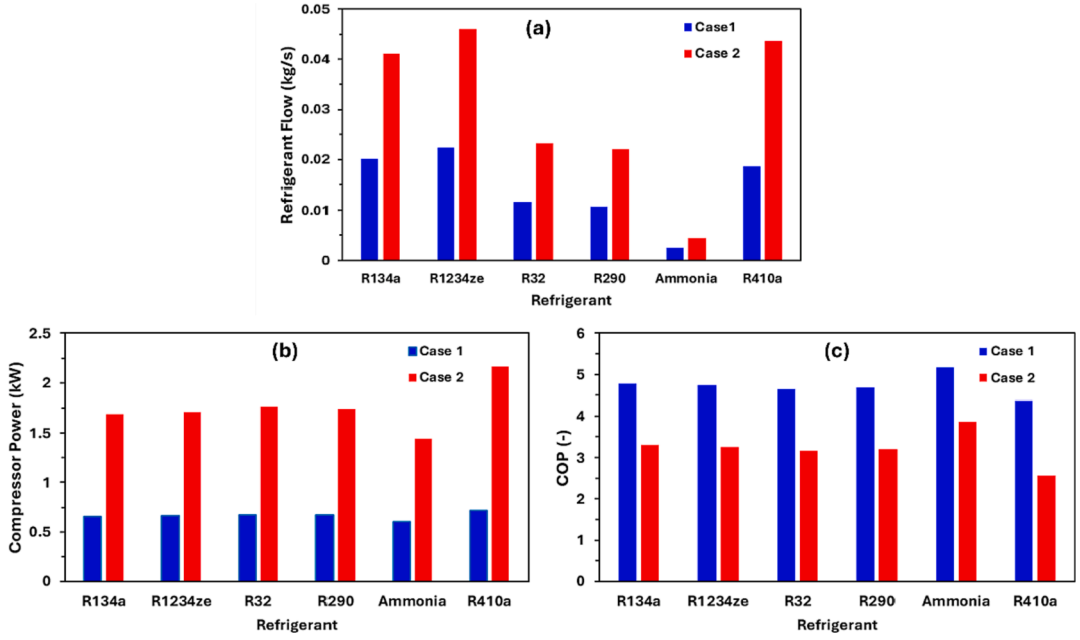

Fig. 3. Influence of six refrigerants on (a) compressor power, (b) COP, and (c) refrigerant mass flow rate for the ASHP. The descriptions of the Cases 1 and 2 are provided in Table 4.

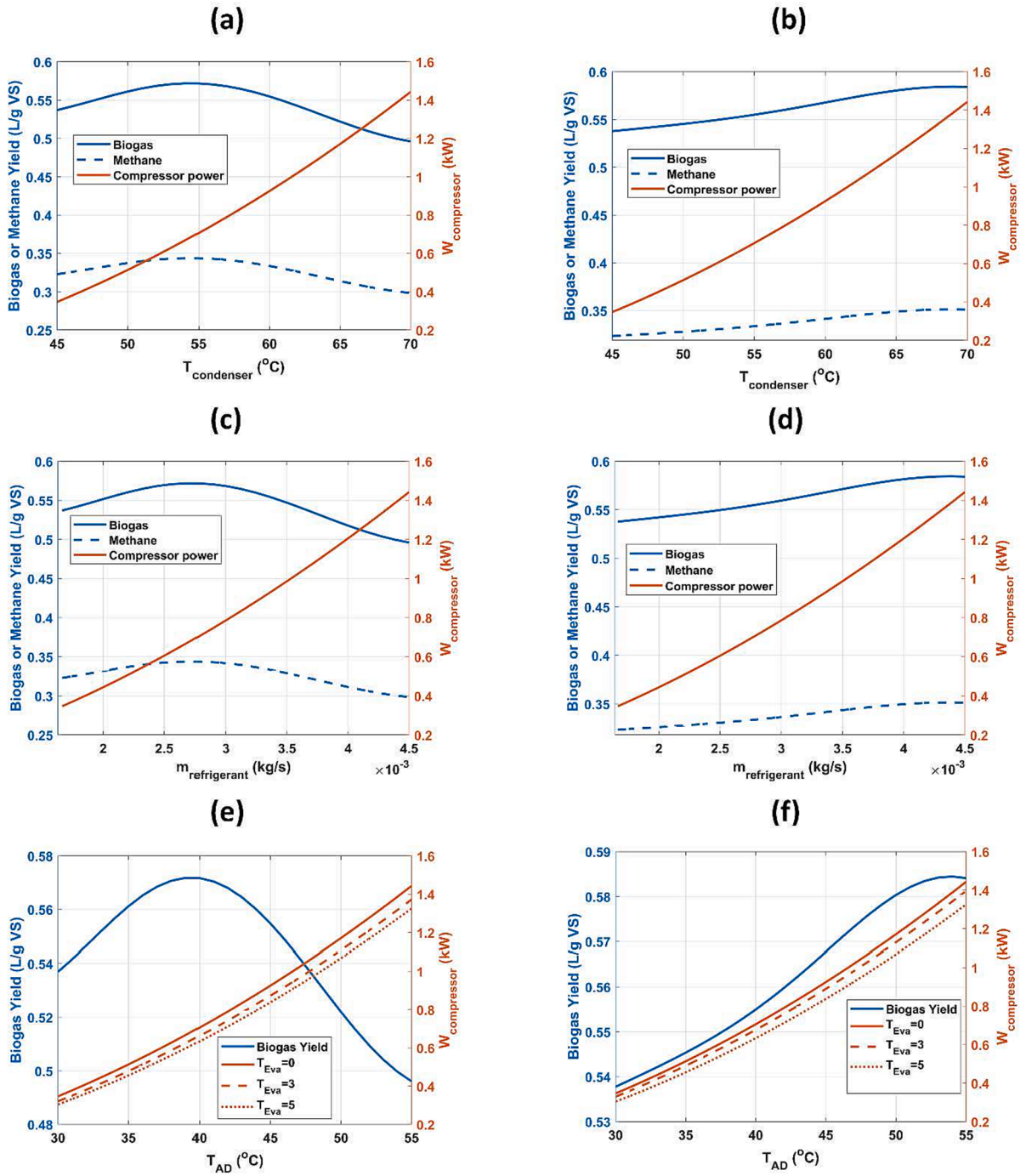

Fig. 4. Results for the parametric sensitivity analysis of HP integrated with the AD system for two scenarios (Case-1 and Case-2). Effect of condenser temperature variation for (a) Case 1 and (b) Case 2. Effect of refrigerant mass flow variation for (c) Case 1 and (d) Case 2. Effect of evaporator temperature for (e) Case 1 and (f) Case 2. Details for different cases are provided in Table 4.

To transfer the required heat that would elevate the temperature of the waste stream (which is within the range of 10–20 °C) to either 37.5 (Case 1) or 55 °C (Case 2), the heat generated by the ASHP condenser is transferred to the AD by means of an external water jacketed coolant loop. The refrigerant flow required, compressor power consumption, and COP to supply these thermal energy demands are shown in Fig. 3a, 3b, and 3c, respectively. Fig. 3a reveals that for both the AD operational cases, using ammonia as a refrigerant would require the lowest amount of flow rate, which are 0.0025 kg/s (Case 1) and 0.0045 kg/s (Case 2). Since the temperature difference between the waste stream and the AD temperature is lower for Case 1 ($\Delta T = 22.5$ °C) than the Case 2 ($\Delta T =$ 40 °C), the Case 1 is attributed to lower refrigerant flow rates. The lower flow rate of refrigerant implies lower pumping power, compact design of the ASHP, and less requirement of tubing, which can ultimately reduce both capital and operational costs. If R410 would have been used as a refrigerant instead of ammonia to produce similar AD performance, the refrigerant mass flow should be 7.4 times higher for Case 1 and 9.4 times higher for Case 2. The benefits of using ammonia as a refrigerant in terms of compressor power reduction and COP improvement can be confirmed from Fig. 3b and c, respectively. For instance, the ASHP utilizing ammonia as the refrigerant can save 15 % and 33 % power as compared to R410a for Cases 1 and 2, respectively.

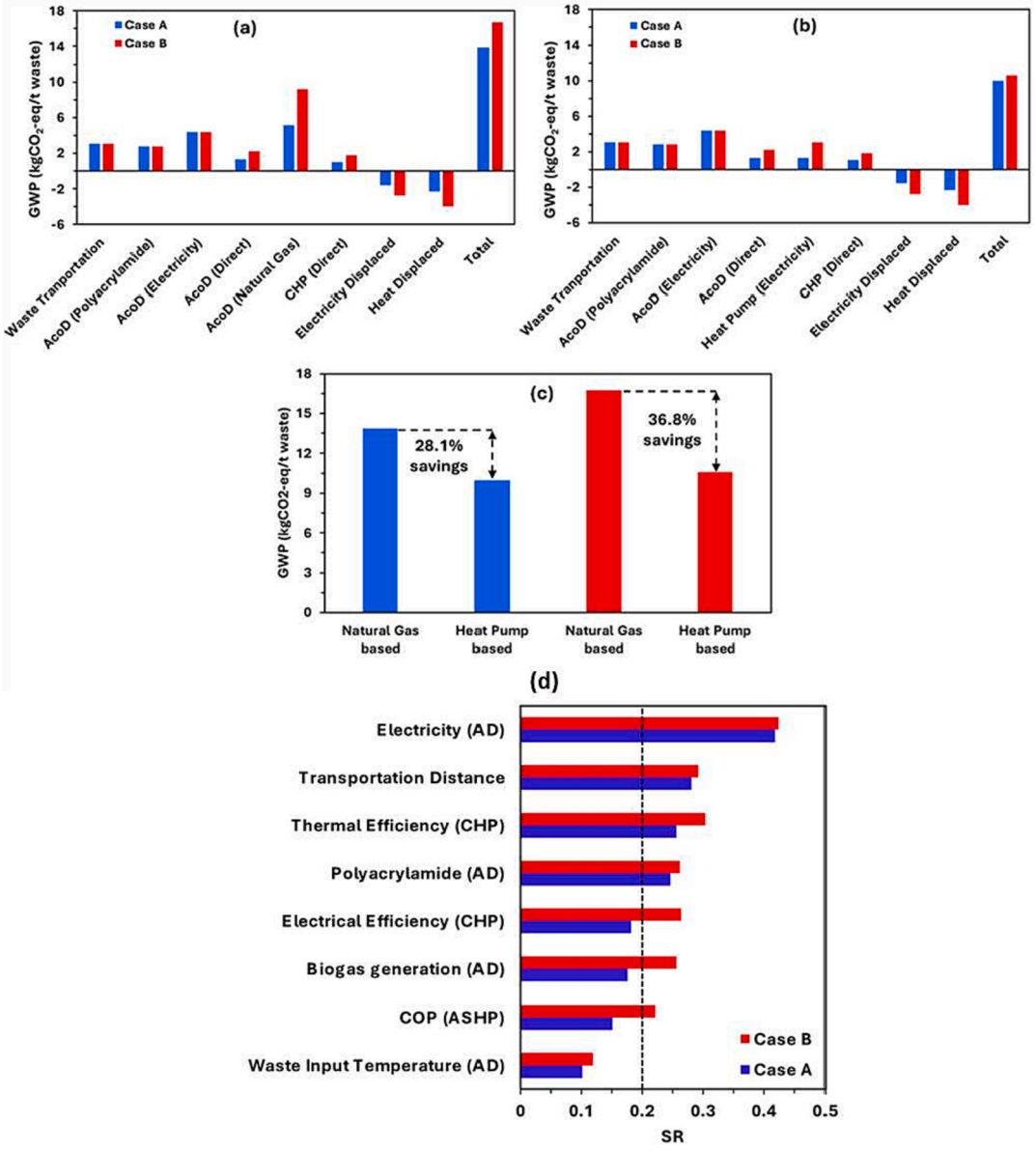

Fig. 5. Stagewise breakdown of GWP for AD with different operating and feedstock conditions. (a) natural gas-based heating for AD, (b) heat pump-based heating for AD, and (c) comparison of both systems with percentage of savings. (d) One-way parametric sensitivity analysis via quantification of SR. The sensitivity map shows the influence of individual parameters on the GWP. The black dotted line corresponds to SR = 0.2, which signifies 6 % change in GWP. The parametric scenarios with SR values below 0.2 have insignificant influence on the GWP. Parametric details for Cases A and B are provided in Table 5.

3.2.2. Influences of condenser Temperature, refrigerant mass Flow, and evaporator temperature

Considering ammonia as the optimal refrigerant of the ASHP, in the subsequent step a sensitivity analysis is performed to select the optimal condenser for the AD operation as shown in Fig. 4a (Case 1) and 4b (Case 1). By varying the condenser temperature, an optimum value of biogas and methane yields are seen at the condenser temperature of 52.5 °C for Case 1 (see Fig. 4a), while that for the Case 2 increases to 70 °C (see Fig. 4b). To provide an elevated condenser temperature, the compressor power consumption increases monotonically. Additionally, to operate near the optimal biogas and methane yield, the Case 1 requires a lower amount of compressor power than that of Case 2. The higher heat demand by the AD requires a higher outlet condenser temperature, which causes more refrigerant to condense in the condenser. Therefore, raising the heat supply temperature would in turn require a higher mass flow of refrigerant to handle the higher heat load. Therefore, for both Fig. 4c and d, the trends closely follow those shown in Fig. 4a and b, respectively.

Similar to refrigerant mass flow, the evaporator temperature has an indirect effect on the ASHP and AD performance (Yu et al., 2022). The parametric variations for Cases 1 and 2 are shown in Fig. 4e and f for three different evaporator temperatures: 0 °C, 3 °C, and 5 °C. For Case 1 (see Fig. 4e), the maximum value of biogas production is approximately 0.556 L gVS^{-1} day^{-1}, which required 0.65 kW compressor power if the evaporator temperature is set to 0 °C. If the evaporator temperature was set to 3 °C or 5 °C, then the compressor power would have reduced to 0.61 kW and 0.56 kW, respectively. This is because raising the evaporator temperature diminishes the heat transfer-related irreversibility of the AHSP and improves the COP of the ASHP (Gupta et al., 2020). A similar inspection of Fig. 4f reveals that for the highest biogas yield of 0.585 L gVS^{-1} day^{-1}, setting the evaporator temperature to 0 °C requires 1.44 kW compressor power.

3.3. Life cycle assessment

Based on the ML-based biogas yield prediction model, thermodynamic model for heat pump, and LCA methodology, the carbon footprint analysis has been conducted. Firstly, the biogas yields were calculated based on the input parameters provided in Table 4. The temperature of the AD system is selected such that it provides the maximum biogas yield corresponding to a certain waste stream parameters (e.g., OLR, VS, HRT). The first case (Case A) is a mesophilic temperature scenario (37.5 °C), while the latter (Case B) corresponds to thermophilic condition with 55 °C. For each of these cases two LCA scenarios are considered where heat to the AD system is supplied by: (a) heat produced from central natural gas grid (for UK context) and (b) heat produced using an on-site ASHP.

Fig. 5a and 5b show the stage-wise GWP breakdown expressed in terms of $kgCO_2$-eq/t feedstock for the natural gas-based and heat pump-based scenarios, respectively. The total environmental footprints for Cases A and B for the natural gas-based system are 13.87 and 16.74 $kgCO_2$-eq/t feedstock, respectively (Edwards et al., 2017; Evangelisti et al., 2014). Case B has a higher carbon footprint than Case A, due to its higher demand for thermal energy to boost the temperature of AD feedstock from 15 °C to 55 °C (i.e., $\Delta T = 40$ °C) (Edwards et al., 2017). In contrast, the case A requires only a $\Delta T = 22.5$ °C, reducing the natural gas based thermal energy requirement. Although a higher ΔT increases the electricity and heat output from the AD process (see Fig. 5a) due to higher biogas production, the input thermal energy requirement offsets the carbon emission gains. This observation is consistent with the recent literature which focuses on the effect of AD temperature on overall process performance (Nie et al., 2021). It is also worth mentioning that related LCA studies often account for the carbon emission offsetting offered by AD when compared to conventional waste disposal methods (e.g., landfill, compositing, or incineration) (Edwards et al., 2017; Evangelisti et al., 2014; Gupta et al., 2022b). This is excluded from the present work due to potential data uncertainty associated with this component.

The carbon footprints for heat pump-based scenario are shown in Fig. 5b, which for Cases A and B are 9.97 and 10.57 $kgCO_2$-eq/t feedstock. In this scenario, the thermal energy required for the AD is supplied by an ASHP operated by electricity. The carbon footprint hotspots for these schemes are direct and indirect emissions for waste transportation (29.5 %), polyacrylamide required by the AD plant (27 %), and electricity consumption for the AD plant (42 %). The components that mitigate the GWP are grid electricity and thermal energy displacement. Overall, it is evident from Fig. 5c that retrofitting a natural gas-based AD heating system by electricity-driven ASHP can mitigate 28.1 % and 36.8 % GWP, when compared to the baseline system. These findings can significantly support future development of carbon footprint mitigation and environment-friendly waste management. It is worthwhile mentioning that the ASHP system can have significantly high capital expenditure. Therefore, to support such projects, government support schemes in the form of carbon incentives for going beyond net-zero would be essential to realize the economic viability of the project.

Fig. 5d reveals the outcome of the one-way sensitivity analysis for the AD integrated with ASHP system for two different operating scenarios described in Table 4. During this analysis each of the input parameters is varied by 30 % and its influence on GWP is assessed via SR metric (Gupta et al., 2022b). A high-level inspection of Fig. 5d suggests that the GWP is more sensitive for Case B than that of Case A. For Case A, the parameters showing a significant impact (i.e., with $SR > 0.2$) are the electricity and polyacrylamide consumptions for AD, the transportation distance from waste source to AD plant, and the thermal efficiency of the CHP plant (Edwards et al., 2017; Evangelisti et al., 2014). For Case B (i.e., thermophilic AD condition) all the parameters except the feedstock temperature show $SR > 0.2$, suggesting that any uncertainties associated with these quantities can significantly impact the GWP results.

4. Conclusions

The research investigated the environmental benefits of heating an anaerobic digestion (AD) process using an air source heat pump (ASHP), a promising solution for tackling extreme ambient temperature variation and achieving net-zero pledge. The optimal machine learning-based biogas yield prediction model achieved $R^2 = 0.84$ with RMSE = 0.0755 L/(gVS-day). A life cycle assessment framework compared the proposed solution to a natural gas-based AD heating system. Findings revealed that the ASHP-based AD systems achieved 28.1% (thermophilic) and 36.8% (mesophilic) reduction in the carbon footprint as compared to the baseline system. Further techno-economic feasibility analysis for such systems would facilitate policymaking and practical implementation.

Declaration of Competing Interest

The authors declare that they have no known competing financial interests or personal relationships that could have appeared to influence the work reported in this paper.

Data availability

A relevant statement is added in the Acknowledgement section.

Acknowledgements

The authors acknowledge the Engineering and Physical Sciences Research Council (EPSRC) Programme Grant (EP/V030515/1). Siming You acknowledges Supergen Bioenergy Hub Rapid Response Funding (RR 2022_10) and Royal Society International Exchange Scheme (EC \NSFC\211175). Rohit Gupta acknowledges the Royal Society Newton International Fellowship (NIF\R1\211013). All data supporting this study are provided in full in this paper. The MATLAB codes for this paper will be provided upon reasonable request. The author has applied a Creative Commons Attribution (CC BY) licence (where permitted by UKRI 'Open Government Licence' or 'Creative Commons Attribution No-derivatives (CC BY-ND)' licence may be stated instead) to any author accepted manuscript version arising.

Appendix A. Supplementary data

Supplementary data to this article can be found online at https://doi.org/10.1016/j.biortech.2022.128485.

References

Almomani, F., 2020. Prediction of biogas production from chemically treated co-digested agricultural waste using artificial neural network. Fuel 280, 118573.
Ascher, S., Li, W., You, S., 2020. Life cycle assessment and net present worth analysis of a community-based food waste treatment system. Bioresour. Technol. 305, 123076.
Ascher, S., Sloan, W., Watson, I., You, S., 2022a. A comprehensive artificial neural network model for gasification process prediction. Appl. Energy 320, 119289.
Ascher, S., Wang, X., Watson, I., Sloan, W., You, S., 2022b. Interpretable machine learning to model biomass and waste gasification. Bioresour. Technol. 364, 128062.
Baskaran, A., Mathews, P.K., 2015. Investigation of new eco friendly refrigerant mixture alternative to R134a in domestic refrigerator. Aust. J. Basic Appl. Sci. 9 (5), 297–306.
Cruz, I.A., Chuenchart, W., Long, F., Surendra, K., Andrade, L.R.S., Bilal, M., Liu, H., Figueiredo, R.T., Khanal, S.K., Ferreira, L.F.R., 2022. Application of machine learning in anaerobic digestion: perspectives and challenges. Bioresour. Technol. 345, 126433.
Edwards, J., Othman, M., Crossin, E., Burn, S., 2017. Anaerobic co-digestion of municipal food waste and sewage sludge: a comparative life cycle assessment in the context of a waste service provision. Bioresour. Technol. 223, 237–249.
Evangelisti, S., Lettieri, P., Borello, D., Clift, R., 2014. Life cycle assessment of energy from waste via anaerobic digestion: a UK case study. Waste Manag. 34 (1), 226–237.
Gupta, R., Asgari, S., Moazamigoodarzi, H., Pal, S., Puri, I.K., 2020. Cooling architecture selection for air-cooled data centers by minimizing exergy destruction. Energy 201, 117625.
Gupta, R., McRoberts, R., Yu, Z., Smith, C., Sloan, W., You, S., 2022a. Life cycle assessment of biodiesel production from rapeseed oil: influence of process parameters and scale. Bioresour. Technol. 360, 127532.

Gupta, R., Miller, R., Sloan, W., You, S., 2022b. Economic and environmental assessment of organic waste to biomethane conversion. Bioresour. Technol. 345, 126500.
Karki, R., Chuenchart, W., Surendra, K., Shrestha, S., Raskin, L., Sung, S., Hashimoto, A., Khanal, S.K., 2021. Anaerobic co-digestion: Current status and perspectives. Bioresour. Technol. 330, 125001.
Kesharwani, N., Bajpai, S., 2020. Batch anaerobic co-digestion of food waste and sludge: a multi criteria decision modelling (MCDM) approach. SN Applied Sciences 2 (8), 1–11.
Kothari, R., Pandey, A., Kumar, S., Tyagi, V., Tyagi, S., 2014. Different aspects of dry anaerobic digestion for bio-energy: An overview. Renew. Sustain. Energy Rev. 39, 174–195.
Li, Y., Gupta, R., You, S., 2022. Machine learning assisted prediction of biochar yield and composition via pyrolysis of biomass. Bioresour. Technol. 359, 127511.
Lombardi, L., Mendecka, B., Fabrizi, S., 2020. Solar integrated anaerobic digester: energy savings and economics. Energies 13 (17), 4292.
Long, F., Wang, L., Cai, W., Lesnik, K., Liu, H., 2021. Predicting the performance of anaerobic digestion using machine learning algorithms and genomic data. Water Res. 199, 117182.
Nie, E., He, P., Zhang, H., Hao, L., Shao, L., Lü, F., 2021. How does temperature regulate anaerobic digestion? Renew. Sustain. Energy Rev. 150, 111453.
Park, J.-G., Jun, H.-B., Heo, T.-Y., 2021. Retraining prior state performances of anaerobic digestion improves prediction accuracy of methane yield in various machine learning models. Appl. Energy 298, 117250.
Pastor, L., Ruiz, L., Pascual, A., Ruiz, B., 2013. Co-digestion of used oils and urban landfill leachates with sewage sludge and the effect on the biogas production. Appl. Energy 107, 438–445.
Polizzi, C., Alatriste-Mondragón, F., Munz, G., 2018. The role of organic load and ammonia inhibition in anaerobic digestion of tannery fleshing. Water Resour. Ind. 19, 25–34.
Şenol, H., 2021. Methane yield prediction of ultrasonic pretreated sewage sludge by means of an artificial neural network. Energy 215, 119173.
Sharma, I., Rackemann, D., Ramirez, J., Cronin, D.J., Moghaddam, L., Beltramini, J.N., Te'o, J., Li, K., Shi, C., Doherty, W.O., 2022. Exploring the potential for biomethane production by the hybrid anaerobic digestion and hydrothermal gasification process: a review. J. Clean. Prod. 132507.
Sudiartha, G.A.W., Imai, T., Hung, Y.-T., 2022. Effects of stepwise temperature shifts in anaerobic digestion for treating municipal wastewater sludge: a genomic study. Int. J. Environ. Res. Public Health 19 (9), 5728.
Sun, C., Guo, L., Zheng, Y., Yu, D., Jin, C., Zhao, Y., Yao, Z., Gao, M., She, Z., 2022. Effect of mixed primary and secondary sludge for two-stage anaerobic digestion (AD). Bioresour. Technol. 343, 126160.
Wang, Y., Huntington, T., Scown, C.D., 2021. Tree-based automated machine learning to predict biogas production for anaerobic co-digestion of organic waste. ACS Sustain. Chem. Eng. 9 (38), 12990–13000.
Xu, W., Long, F., Zhao, H., Zhang, Y., Liang, D., Wang, L., Lesnik, K.L., Cao, H., Zhang, Y., Liu, H., 2021. Performance prediction of ZVI-based anaerobic digestion reactor using machine learning algorithms. Waste Manag. 121, 59–66.
Xu, R., Zhang, K., Liu, P., Khan, A., Xiong, J., Tian, F., Li, X., 2018. A critical review on the interaction of substrate nutrient balance and microbial community structure and function in anaerobic co-digestion. Bioresour. Technol. 247, 1119–1127.
Yu, Z., McKeown, A., Hajabdollahi Ouderji, Z., Essadik, M., 2022. A flexible heat pump cycle for heat recovery. Commun. Eng. 1 (1), 1–12.